Geometric studies on variable radius spiral cone-beam scanning

Yangbo Ye[a)] and Jiehua Zhu
Department of Mathematics, The University of Iowa, Iowa City, Iowa 52242

Ge Wang
Department of Radiology, The University of Iowa, Iowa City, Iowa 52242

(Received 20 November 2003; revised 21 February 2004; accepted for publication 31 March 2004; published 24 May 2004)

The goal is to perform geometric studies on cone-beam CT scanning along a three-dimensional (3D) spiral of variable radius. First, the background for variable radius spiral cone-beam scanning is given in the context of electron-beam CT/micro-CT. Then, necessary and sufficient conditions are proved for existence and uniqueness of PI lines inside the variable radius 3D spiral. These results are necessary steps toward exact cone-beam reconstruction from a 3D spiral scan of variable radius, adapting Katsevich's formula for the standard helical cone-beam scanning. It is shown in the paper that when the longitudinally projected planar spiral is not always convex toward the origin, the PI line may not be unique in the envelope defined by the tangents of the spiral. This situation can be avoided by using planar spirals whose curvatures are always positive. Using such a spiral, a longitudinally homogeneous region inside the corresponding 3D spiral is constructed in which any point is passed by one and only one PI line, provided the angle ω between planar spiral's tangent and radius is bounded by $|\omega-90°|\leqslant\varepsilon$ for some positive $\varepsilon\leqslant 32.48°$. If the radius varies monotonically, this region is larger and one may allow $\varepsilon\leqslant 51.85°$. Examples for 3D spirals based on logarithmic and Archimedean spirals are given. The corresponding generalized Tam–Danielsson detection windows are also formulated. © *2004 American Association of Physicists in Medicine.* [DOI: 10.1118/1.1751251]

Key words: electron-beam CT, micro-CT, cone-beam, spiral scanning, generalized Tam–Danielsson detection window, PI line

I. BACKGROUND

Using the proprietary technology, electron-beam CT scanners[1] are quite different from the main stream mechanical CT scanners.[2] Most distinctively, electron-beam CT scanners allow scan times down to 50 ms. In the EBCT design, an electron beam is focused on one of tungsten arcs of 210° beneath the patient. The electron beam is electromagnetically steered to produce fan-beam projections continuously on detector arrays above the patient. In addition to its remarkable applications for dynamic imaging of cardiac structures, EBCT is also a powerful tool for physiological imaging. However, in our opinion there are two major weaknesses with the current EBCT techniques. First, it is not in cone-beam geometry and does not support spiral/helical scanning, while it has become clear that spiral/helical cone-beam scanning is advantageous for the next generation of biomedical CT to solve the so-called long object problem. Second, the x-ray spot is not sufficiently intensive to produce the image quality the mechanical rotation based scanners can achieve.

Just as we need tomographic equipment in patient studies, we also need micro-tomographic devices in small animal studies.[3] Although there has been an explosive growth in the development of micro-CT scanners, much of the efforts have been limited to high spatial resolution. In the 1990s, a number of micro-CT systems were constructed. Most of these systems employ CCD cameras, micro-focus x-ray tubes, and have image resolutions between 20 and 100 μm. In recent prototypes of micro-CT systems, the data acquisition system rotates about an animal table, while in earlier systems an animal stage is rotated in a fixed data acquisition system. These imaging systems produce down to a few micron resolution images, and permit screening of small animals for mutations or pathologies, and monitoring of disease progression and response to therapy. However, to date there is no major effort devoted to development of a micro-CT scanner that allows ultrafast *in vivo* imaging to study dynamic processes. As a primary example, cardiac micro-CT of the mouse is simply impossible with the state of the art of the technology.

In 1991, Wang *et al.* proposed a nonstandard spiral cone-beam algorithm to solve the long object problem.[4] However, their algorithm is of Feldkamp-type and only produces approximate results. In 2002 and 2003, Katsevich proposed an exact helical cone-beam algorithm,[5–7] which is a quantum leap relative to the earlier algorithms.[4,8–11]

The Katsevich helical cone-beam method is formulated in terms of the PI line and the Tam–Danielsson window. It has been proved[10,11] that for any object point inside a scanning helix there is one and only straight line that (1) contains the object point and (2) intersects a helical scanning turn twice. The line segment defined by the two intersections is referred to as the PI line. On the other hand, with the so-called Tam–Danielsson window,[10,12] from any x-ray source only those rays that locate between the immediately upper and lower helical turns are selected. Inspired by the Orlov theorem,[13]

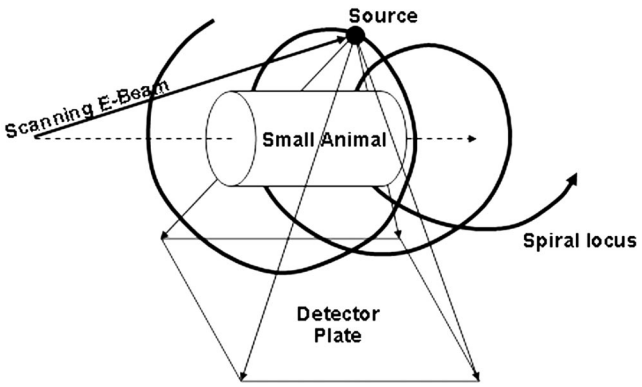

FIG. 1. Conceptual design of electron-beam micro-CT using variable radius cone-beam scanning.

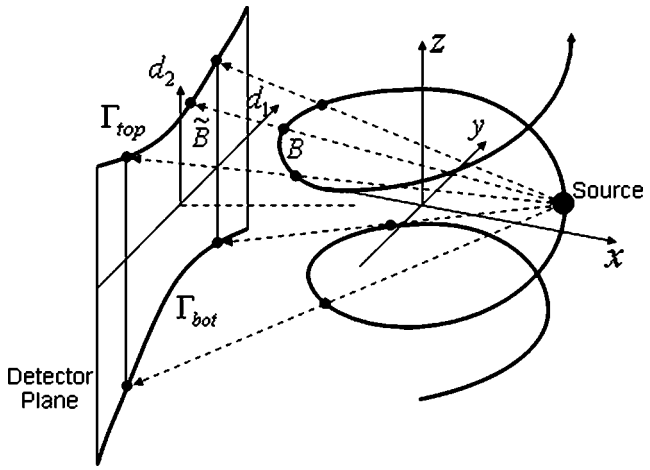

FIG. 2. Generalized Tam–Danielsson detection window delimited by the projected upper and lower turns of the spiral locus.

Dannielsson made the conjecture that cone-beam data collected within the Tam–Dannielsson window along a helical scanning arc delimited by the PI line are sufficient for reconstruction of any object point on the PI line.[10] The Katsevich helical cone-beam formulation can be considered as having proved the Dannielsson conjecture except for a need to use a small amount of data outside the Tam–Danielsson window. Recently, Zou and Pan have reported that such a need can be eliminated in the Katsevich framework.[14] However, Katsevich-type algorithms are currently unavailable for exact image reconstruction with nontrivial spiral cone-beam scanning.

In this paper, we propose to upgrade the EBCT design with a spiral cone-beam scanning capability and adapt the architecture for small animal imaging, especially for cardiac studies of the mouse. The overall concept is shown in Fig. 1, in which the x-ray spot traces a nonstandard spiral locus with the detection coverage defined by a generalized Tam–Danielsson window. In the following after introducing notations in Sec. II, we first describe a minimal detection window for our case in Sec. III, generalizing the standard Tam–Danielsson windows. Then, in Sec. IV we study planar spirals. The results are useful in Secs. V–VII to obtain necessary and sufficient conditions on three-dimension (3D) spirals such that there is one and only one PI line pass through a point inside the 3D spiral. In Secs. VIII–X, examples of 3D spirals with monotone radii and regions with PI line uniqueness are given. Finally in Sec. XI, we discuss a few of relevant issues and directions for further research.

II. NOTATION

Consider a two-dimensional spiral $\rho=R(s)$ in polar coordinates:

$$x=R(s)\cos s, \tag{2.1}$$

$$y=R(s)\sin s, \tag{2.2}$$

where $\rho=\sqrt{x^2+y^2}$. We assume that $R(s)>0$ for any s, and assume that at any s, $R'(s)$ exists. From $\rho=R(s)$ we build a 3D spiral with constant pitch $h>0$:

$$x=R(s)\cos s, \tag{2.3}$$

$$y=R(s)\sin s, \tag{2.4}$$

$$z=hs. \tag{2.5}$$

Let (x_0,y_0,z_0) be a point inside this 3D spiral. A PI line of this point is a line passing through (x_0,y_0,z_0), $(x(s_1),y(s_1),z(s_1))$ and $(x(s_2),y(s_2),z(s_2))$, such that $0<s_2-s_1<2\pi$. The existence and uniqueness of a PI line passing through (x_0,y_0,z_0) is equivalent to the condition that

$$x_0=tx(s_1)+(1-t)x(s_2), \tag{2.6}$$

$$y_0=ty(s_1)+(1-t)y(s_2), \tag{2.7}$$

$$z_0=ths_1+(1-t)hs_2, \tag{2.8}$$

have one and only solution (t,s_1,s_2) with $0<t<1$, $0<s_2-s_1<2\pi$.

III. MINIMUM DETECTION WINDOW

Minimum detection windows for a standard helix, called Tam–Danielsson windows,[10,11] have been used in both approximate and exact cone-beam reconstruction algorithms. Consider a 3D spiral with a variable radius in Eqs. (2.3)–(2.5). In this case, we define the generalized Tam–Danielsson detection window at s_0 as the region in the detector plane bounded by the cone beam projections of the upper and lower turns of the 3D spiral starting from the point S on the 3D spiral corresponding to s_0, where the detector plane is perpendicular to the xy plane, on the opposite side of the origin, and of distance R to the origin. We assume that $R>R(s)$. Figure 2 illustrates the geometry for such a detection window. On the detector plane, any object point within the two consecutive turns is projected onto the region between Γ_{top} and Γ_{bot}, the boundaries of the detector plane. Now we deduce the boundary equations of Γ_{top} and Γ_{bot} for x-ray source at s_0. Let $B=(R(s)\cos s,R(s)\sin s,hs)$ be any point on the turn of the 3D spiral immediately above or

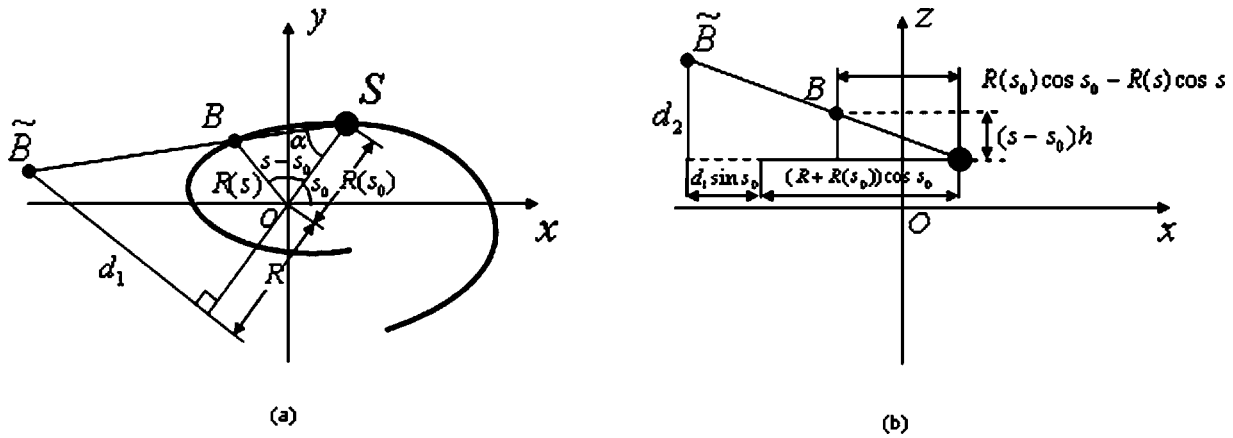

FIG. 3. Views of projected trajectory of the helical locus. (a) View for the computation of the d_1, (b) view for the computation of the d_2.

below s_0, and $\tilde{B}$ the cone beam projection of B on the detector plane. The top and front views of the geometry are given in Fig. 3.

On the xy plane, we have

$$\frac{R(s)}{\sin\alpha}=\frac{BS}{\sin(s-s_0)}$$

and

$$BS^2=R(s_0)^2+R(s)^2-2R(s_0)R(s)\cos(s-s_0),$$

where we only consider the case of $-\pi/2<\alpha<\pi/2$. Then

$$\sin\alpha=\frac{R(s)}{BS}\sin(s-s_0)$$

and

$$\tan\alpha=\frac{\sin\alpha}{\sqrt{1-\sin^2\alpha}}=\frac{R(s)\sin(s-s_0)}{\sqrt{BS^2-R(s)^2\sin^2(s-s_0)}}$$
$$=\frac{R(s)\sin(s-s_0)}{R(s_0)-R(s)\cos(s-s_0)}.$$

Therefore,

$$d_1=(R+R(s_0))\tan\alpha=\frac{R(s)(R+R(s_0))\sin(s-s_0)}{R(s_0)-R(s)\cos(s-s_0)}. \tag{3.1}$$

On the xz plane,

$$\frac{(s-s_0)h}{R(s_0)\cos s_0-R(s)\cos s}=\frac{d_2}{(R+R(s_0))\cos s_0+d_1\sin s_0}.$$

Consequently,

$$d_2=(s-s_0)h\frac{(R+R(s_0))\cos s_0+d_1\sin s_0}{R(s_0)\cos s_0-R(s)\cos s}$$
$$=\frac{(R+R(s_0))(s-s_0)h}{R(s_0)-R(s)\cos(s-s_0)}. \tag{3.2}$$

Equations (3.1) and (3.2) are therefore boundary equations in parametric forms for our generalized Tam–Danielsson detection window. Since we assume that $-\pi/2<\alpha<\pi/2$, the parameter s is taken over $(s_0-2\pi,s_0)$ and $(s_0,s_0+2\pi)$ satisfying

$$R(s_0)-R(s)\cos(s-s_0)>0.$$

IV. PLANAR SPIRAL

Let $\rho=R(s)$ be a planar spiral in polar coordinates as shown in Fig. 4. Denote by ω the angle between OM and the tangent at M. Then

$$\tan\omega=\frac{R(s)}{R'(s)}. \tag{4.1}$$

In fact, the slope of the tangent MN is $\tan\beta=dy/dx$. Then

$$\tan\omega=\tan(\beta-s)=\frac{\tan\beta-\tan s}{1+\tan\beta\tan s}$$
$$=\frac{\dfrac{dy}{dx}-\dfrac{y}{x}}{1+\dfrac{dy}{dx}\cdot\dfrac{y}{x}}=\frac{x\dfrac{dy}{ds}-y\dfrac{dx}{ds}}{x\dfrac{dx}{ds}+y\dfrac{dy}{ds}}.$$

From $R(s)^2=x^2+y^2$, we get

$$R(s)R'(s)=x\frac{dx}{ds}+y\frac{dy}{ds},$$

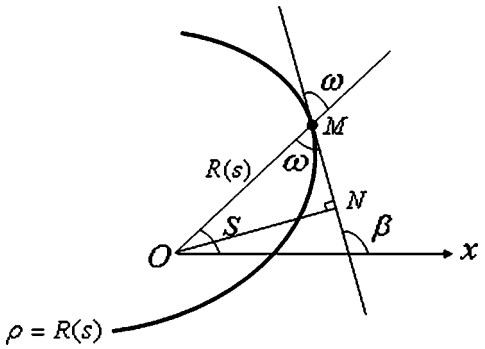

FIG. 4. Geometry of a planar spiral.

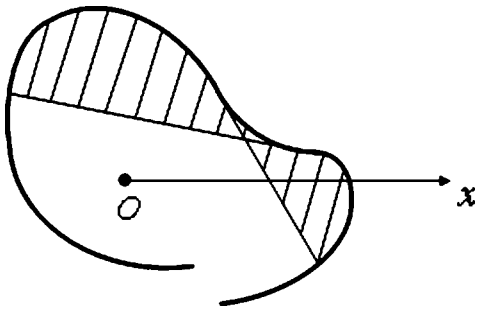

FIG. 5. A shaded region.

and hence by Eqs. (2.1) and (2.2)

$$\tan\omega=\frac{1}{R(s)R'(s)}(R(s)\cos s(R'(s)\sin s+R(s)\cos s)$$

$$-R(s)\sin s(R'(s)\cos s-R(s)\sin s))=\frac{R(s)}{R'(s)}.$$

From Eq. (4.1) we can compute the distance between the tangent MN and the origin O:

$$\overline{ON}=R(s)\sin\omega=R(s)\cdot\frac{|\tan\omega|}{\sqrt{1+\tan^2\omega}}=\frac{R^2(s)}{\sqrt{R(s)^2+R'(s)^2}}. \tag{4.2}$$

Theorem 4.1: *Let (x_0,y_0) be a point inside the planar spiral $\rho=R(s)$. A necessary and sufficient condition that for any given s_1 there is unique s_2 and t, and for given s_2 there is unique s_1 and t, satisfying Eqs. (2.6) and (2.7) with $0<t<1$ and $0<s_2-s_1<2\pi$, is that (x_0,y_0) is on the inside of every tangent of the planar spiral for s in an interval of length 2π.*

Proof: If (x_0,y_0) is in the shaded region shown in Fig. 5, the outside of a tangent line, then there is a line passing through (x_0,y_0) which intersects the planar spiral at more than two points. This will violate the uniqueness of s_1 or s_2. On the other hand, if (x_0,y_0) is not in the shaded region inside the planar spiral, any line passing through (x_0,y_0) will only intersect the curve at two points.

If the object region is a disk centered at the origin as shown in Fig. 6, we can use Eq. (4.2) to determine the maximum radius with uniqueness.

Theorem 4.2: *Let I be an interval of length 2π. The maximum radius r such that any line passing through any point (x_0,y_0) in the disk $x^2+y^2<r^2$ intersects the planar spiral for $s\in I$ at two and only two points is*

$$r=\min_{s\in I}\frac{R(s)^2}{\sqrt{R(s)^2+R'(s)^2}}. \tag{4.3}$$

The curvature of the planar curve $\rho=R(s)$ at s is given by

$$\kappa=\frac{R(s)^2+2R'(s)^2-R(s)R''(s)}{(R(s)^2+R'(s)^2)^{3/2}}. \tag{4.4}$$

If κ is always non-negative, the curve is convex toward the origin, and any point (x_0,y_0) inside $\rho=R(s)$ satisfies the condition in Theorem 4.1.

Theorem 4.3: *Assume that $R(s)$ has second derivative and*

$$R(s)^2+2R'(s)^2-R(s)R''(s)\geqslant 0 \tag{4.5}$$

at any s in an interval of length 2π. Then for any point (x_0,y_0) inside the planar spiral, a line passing through (x_0,y_0) intersects the planar spiral over I at two and only two points.

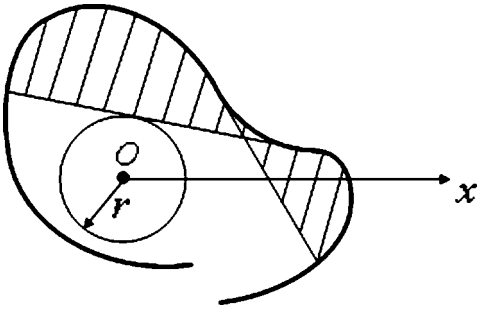

FIG. 6. A disk.

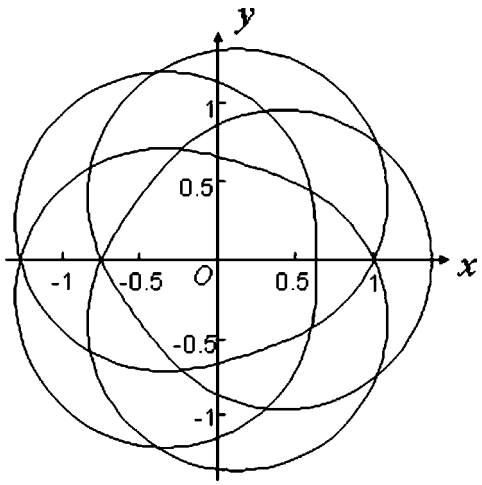

FIG. 7. Graph of $\rho=1+(15/41)\cos(5s/4)$.

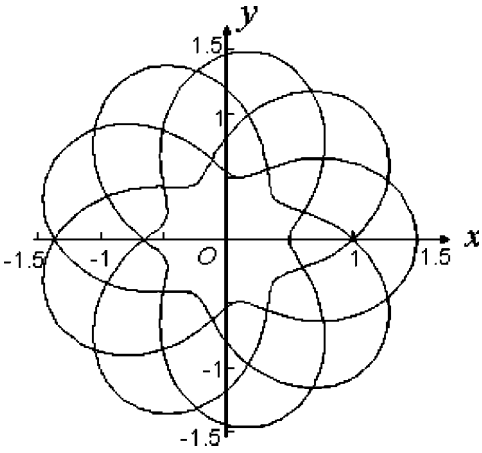

FIG. 8. Graph of $\rho=1+(1/2)\cos(9s/4)$.

In fact, since the curvature (4.4) is always non-negative, the tangent lines of the planar spiral are always outside the curve.

In the following sections, we will always assume that the planar spiral $\rho=R(s)$ has non-negative curvature, satisfying Eq. (4.5). In Fig. 7, the graph of $\rho=1+(15/41)\cos(5s/4)$ is given. Its curvature is always positive. Figure 8 shows the graphs of the function $\rho=1+(1/2)\cos(9s/4)$ where the curvature is negative at some s.

V. EXISTENCE OF PI LINE

Now we turn to the third equation (2.8). Fix a point (x_0,y_0) in the region determined by Theorem 4.3. Then to every s_1 there is unique t and s_2 satisfying Eqs. (2.6) and (2.7), with $0<t<1$ and $0<s_2-s_1<2\pi$. Therefore t and s_2 are functions of s_1, and hence

$$z=ths_1+(1-t)hs_2 \tag{5.1}$$

is also a function of s_1. Denote this latter function by $z(s_1)$.

Assume that our 3D spiral (2.6)–(2.8) is taken over $s\in[a,b]$. The existence of PI lines passing through a point (x_0,y_0,z_0) is equivalent to saying that there is $s_1\in[a,b]$ such that the continuous function (5.1) assumes z_0 as a function value: $z_0=z(s_1)$.

Theorem 5.1: *Let $\rho=R(s)$, $z=hs$, be a 3D spiral for $s\in[a,b]$ with $b-a>4\pi$. Assume Eq. (4.5) for any $s\in[a,b]$. For any point (x_0,y_0,z_0) inside the 3D spiral with*

$$(a+2\pi)h\leqslant z_0\leqslant(b-2\pi)h, \tag{5.2}$$

there exists a π line passing through (x_0,y_0,z_0).

Proof: Take $s_1=a$ and determine the unique t and s_2 by Eqs. (2.6) and (2.7) with $0<t<1$ and $0<s_2-s_1<2\pi$. Then $z(a)=tha+(1-t)hs_2<(a+2\pi)h$. On the other hand take $s_1=b-2\pi$, then find unique t and s_2 satisfying Eqs. (2.6) and (2.7). Again $0<t<1$ and $0<s_2-s_1<2\pi$. Then $z(b-2\pi)>(b-2\pi)h$. By Eq. (5.2), z_0 is between these two function values $z(a)<z_0<z(b-2\pi)$. Consequently there is $s_1\in[a,b-2\pi]$ such that $z_0=z(s_1)$, because $z(s_1)$ is continuous.

VI. FIRST DERIVATIVE OF $z(s_1)$

To study the uniqueness of PI line, we want to differentiate z with respect to s_1:

$$\frac{dz}{ds_1}=(s_1-s_2)h\frac{dt}{ds_1}+(1-t)h\frac{ds_2}{ds_1}+th. \tag{6.1}$$

The PI line is unique if and only if dz/ds_1 is always $\geqslant 0$. We compute dt/ds_1 and ds_2/ds_1 by implicit differentiation. Differentiating Eqs. (2.6) and (2.7), we get

$$(x(s_1)-x(s_2))\frac{dt}{ds_1}+(1-t)x'(s_2)\frac{ds_2}{ds_1}=-tx'(s_1),$$

$$(y(s_1)-y(s_2))\frac{dt}{ds_1}+(1-t)y'(s_2)\frac{ds_2}{ds_1}=-ty'(s_1).$$

Solving these linear equations for dt/ds_1 and ds_2/ds_1, we have

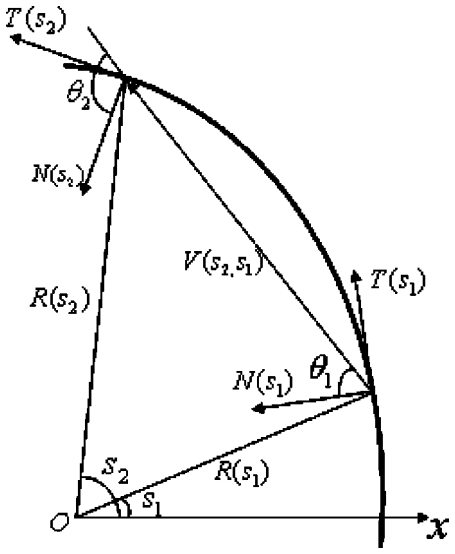

FIG. 9. Geometry of the vectors $V(s_2,s_1)$, $T(s_1)$, $N(s_1)$, $T(s_2)$, and $N(s_2)$.

$$\frac{dt}{ds_1}=t\frac{x'(s_2)y'(s_1)-x'(s_1)y'(s_2)}{y'(s_2)(x(s_1)-x(s_2))-x'(s_2)(y(s_1)-y(s_2))}, \tag{6.2}$$

$$\frac{ds_2}{ds_1}=\frac{t}{1-t}\frac{x'(s_1)(y(s_1)-y(s_2))-y'(s_1)(x(s_1)-x(s_2))}{y'(s_2)(x(s_1)-x(s_2))-x'(s_2)(y(s_1)-y(s_2))}. \tag{6.3}$$

For the plane spiral in Eqs. (2.1) and (2.2), $T(s)=(x'(s),y'(s))$ is a tangent vector at s. Denote by $N(s)=(-y'(s),x'(s))$ a norm vector pointing inward at s, and by

$$V(s_2,s_1)=(x(s_2)-x(s_1),y(s_2)-y(s_1))$$

the vector along the PI line from the point $(x(s_1),y(s_1))$ to the point $(x(s_2),y(s_2))$. Then

$$\frac{dt}{ds_1}=-t\frac{T(s_2)N(s_1)}{N(s_2)V(s_2,s_1)},$$

$$\frac{ds_2}{ds_1}=-\frac{t}{1-t}\frac{N(s_1)V(s_2,s_1)}{N(s_2)V(s_2,s_1)},$$

and

$$\frac{dz}{ds_1}=th\left(1+(s_2-s_1)\frac{T(s_2)N(s_1)}{N(s_2)V(s_2,s_1)}-\frac{N(s_1)V(s_2,s_1)}{N(s_2)V(s_2,s_1)}\right)$$

$$=\frac{th}{N(s_2)V(s_2,s_1)}((N(s_2)-N(s_1))\cdot V(s_2,s_1)+(s_2-s_1)T(s_2)N(s_1)). \tag{6.4}$$

VII. UNIQUENESS OF PI LINE

Denote by θ_j the angle from $V(s_2,s_1)$ to $N(s_j)$ (Fig. 9). Since we assume that the point (x_0,y_0), which is on the PI line in the direction of $V(s_2,s_1)$, is in the region given by Theorem 4.3, we know that

$$-\pi/2<\theta_1<\pi/2, \quad \pi/2<\theta_2<3\pi/2. \tag{7.1}$$

Therefore,

$$N(s_2)V(s_2,s_1)<0, \quad N(s_1)V(s_2,s_1)>0, \tag{7.2}$$

and we know that $dz/ds_1 \geqslant 0$ is equivalent to

$$(N(s_1)-N(s_2))V(s_2,s_1)-(s_2-s_1)T(s_2)N(s_1)\geqslant 0. \tag{7.3}$$

Since $x'(s)=R'(s)\cos s-R(s)\sin s$ and $y'(s)=R'(s)\sin s+R(s)\cos s$, Eq. (7.3) is the same as

$$\begin{aligned}&R(s_1)^2+R(s_2)^2-R(s_1)R(s_2)(2\cos(s_2-s_1)\\&\quad+(s_2-s_1)\sin(s_2-s_1))+R'(s_1)R(s_2)(\sin(s_2-s_1)\\&\quad-(s_2-s_1)\cos(s_2-s_1))+R(s_1)R'(s_2)\\&\quad\times(-\sin(s_2-s_1)+(s_2-s_1)\cos(s_2-s_1))\\&\quad-R'(s_1)R'(s_2)(s_2-s_1)\sin(s_2-s_1)\geqslant 0.\end{aligned}$$

Since $R(s)>0$, this is equivalent to

$$\begin{aligned}&\left(\sqrt{\frac{R(s_1)}{R(s_2)}}-\sqrt{\frac{R(s_2)}{R(s_1)}}\right)^2+2-2\cos u-u\sin u\\&\quad+\left(\frac{R'(s_1)}{R(s_1)}-\frac{R'(s_2)}{R(s_2)}\right)(\sin u-u\cos u)\\&\quad-\frac{R'(s_1)}{R(s_1)}\cdot\frac{R'(s_2)}{R(s_2)}u\sin u\geqslant 0,\end{aligned} \tag{7.4}$$

where $u=s_2-s_1$ with $0\leqslant u\leqslant 2\pi$. This gives a proof of the following theorem.

Theorem 7.1: *For a 3D spiral $\rho=R(s)$, $z=hs$, on $s\in[a,b]$, we assume Eq. (4.5) for any s. For any point (x_0,y_0,z_0) inside the 3D spiral with Eq. (5.2) there is one and only one PI line passing through (x_0,y_0,z_0), if and only if Eq. (7.4) holds for all s_1, $s_2\in[a,b]$ with $u=s_2-s_1$, $0\leqslant u\leqslant 2\pi$.*

VIII. SPIRALS WITH MONOTONIC $R(s)$

A. Circle $\rho=R(s)=R$

Note that $2-2\cos u-u\sin u\geqslant 0$ for $0\leqslant u\leqslant 2\pi$. Therefore, if the radius function $R(s)=R$ is constant, the left side of (7.4) becomes $2-2\cos u-u\sin u\geqslant 0$. Consequently Theorem 7.1 holds for the usual helix of constant radius $R(s)=R$.

B. Logarithmic spiral $\rho=R(s)=e^{rs}$

By Eq. (4.1), we know that

$$\frac{R'(s)}{R(s)}=\cot\omega, \tag{8.1}$$

where ω is the angle between the ray from the origin to the point $\rho=R(s)$ on the planar spiral and the tangent vector $T(s)$. If $\rho=R(s)=e^{rs}$ is a logarithmic spiral, $r\neq 0$, then $R'(s)/R(s)=r$ is constant. Consequently for this logarithmic spiral

$$\frac{R'(s_1)}{R(s_1)}-\frac{R'(s_2)}{R(s_2)}=0, \tag{8.2}$$

and the left-hand side of Eq. (7.4) equals

$$e^{ru}+e^{-ru}-(2\cos u+u\sin u)-r^2u\sin u\geqslant 0$$

for $u\in[0,2\pi]$. Therefore for logarithmic spirals, Theorem 7.1 also holds and PI lines are unique inside the 3D spiral.

C. Archimedean spiral $\rho=R(s)=as+b$

We now consider the case that $R(s)=as+b$ is a linear function. To show that it satisfies the condition (7.4) of Theorem 7.1, we may assume that $s_1=0$, $0\leqslant s_2=u\leqslant 2\pi$, $b>0$, and $2\pi a+b>0$. Then

$$\begin{aligned}\left(\sqrt{\frac{R(s_1)}{R(s_2)}}-\sqrt{\frac{R(s_2)}{R(s_1)}}\right)^2&=\frac{b}{au+b}+\frac{au+b}{b}-2\\&=\frac{a^2u^2}{b(au+b)}\end{aligned}$$

and

$$\begin{aligned}\frac{R'(s_1)}{R(s_1)}-\frac{R'(s_2)}{R(s_2)}=\frac{R'(0)}{R(0)}-\frac{R'(u)}{R(u)}&=\frac{a}{b}-\frac{a}{au+b}\\&=\frac{a^2u}{b(au+b)}.\end{aligned}$$

Consequently,

$$\begin{aligned}&\left(\frac{R'(s_1)}{R(s_1)}-\frac{R'(s_2)}{R(s_2)}\right)(\sin u-u\cos u)-\frac{R'(s_1)}{R(s_1)}\frac{R'(s_2)}{R(s_2)}u\sin u\\&\quad=\frac{a^2u}{b(au+b)}(\sin u-u\cos u)-\frac{a^2u}{b(au+b)}\sin u\\&\quad=-\frac{a^2u^2}{b(au+b)}\cos u\end{aligned}$$

and the left-hand side side of Eq. (7.4) becomes

$$2-2\cos u-u\sin u+\frac{a^2u^2}{b(au+b)}(1-\cos u)\geqslant 0.$$

This proves that Theorem 7.1 holds for linear $R(s)$.

IX. UNIQUE PI-LINE REGION FOR GENERAL $R(s)$

For a general function $R(s)$ we cannot expect a full cancellation as in Eq. (8.2). In Fig. 10, the graphs of functions $2-2\cos u-u\sin u$, $\sin u-u\cos u$, and $-u\sin u$ are given. When $R'(s_1)/R(s_1)-R'(s_2)/R(s_2)$ is positive and but small for $s_2-s_1=u$ large, the dip of $\sin u-u\cos u$ near $u=2\pi$ will prevent Eq. (7.4) from being true. This situation can be seen in Fig. 11, the graph on the left-hand side of Eq. (7.4) for $R(s)=1+(15/41)\cos(5s/4)$ for $s_1=0$ and $u=s_2-s_1$ in $[0,2\pi]$.

Similarly, the dip of $-u\sin u$ near $u=2$ may also cause the left-hand side of Eq. (7.4) to be negative.

If we can limit the angle of the tangent vector to be not too steep, we may obtain a cylindrical region $B_r=\{(x_0,y_0,z_0)|x_0^2+y_0^2\leqslant r^2,(a+2\pi)h\leqslant z_0\leqslant(b-2\pi)h\}$ in

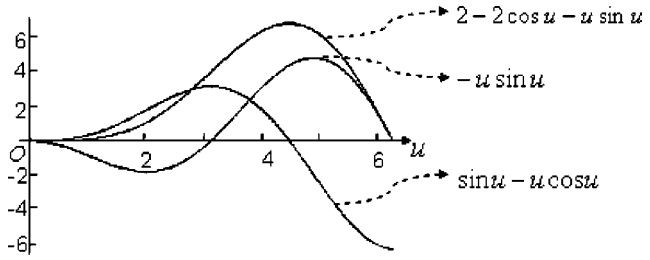

FIG. 10. Plots of $2-2\cos u-u\sin u$ $\sin u-u\cos u$, and $-u\sin u$.

which any point was passed by one and only one PI line.

By Eq. (8.1), a bound for $R'(s)/R(s)$,

$$\left|\frac{R'(s)}{R(s)}\right|\leqslant\varepsilon, \tag{9.1}$$

means that $|\cot\omega|\leqslant\varepsilon$, i.e.,

$$|\omega-\pi/2|\leqslant\tan^{-1}\varepsilon. \tag{9.2}$$

If we take $u=\pi$, then the left-hand side of Eq. (7.4) becomes

$$\left(\sqrt{\frac{R(s_1)}{R(s_2)}}-\sqrt{\frac{R(s_2)}{R(s_1)}}\right)^2+4+\pi\left(\frac{R'(s_1)}{R(s_1)}-\frac{R'(s_2)}{R(s_2)}\right)$$
$$\geqslant 4-2\varepsilon\pi. \tag{9.3}$$

Therefore if $\varepsilon=2/\pi$, i.e., if

$$\left|\omega-\frac{\pi}{2}\right|\leqslant\tan^{-1}\frac{2}{\pi}\cong 0.567\cong 32.48°, \tag{9.4}$$

Eq. (7.4) holds for any point $(0,0,z_0)$.

A smaller ε in Eqs. (9.1) and (9.2) will give us a larger region with PI line uniqueness. Given $\varepsilon\leqslant 2/\pi$ with Eq. (9.1) or equivalently Eq. (9.2), Eq. (7.4) holds if

$$2-2\cos u-u\sin u-2\varepsilon|\sin u-u\cos u|-\varepsilon^2|u\sin u|\geqslant 0. \tag{9.5}$$

Solving its equality for ε, we get

$$\varepsilon=\frac{1}{u|\sin u|}(-|\sin u-u\cos u|$$
$$+\sqrt{(\sin u-u\cos u)^2+u|\sin u|(2-2\cos u-u\sin u)}) \tag{9.6}$$

for $0\leqslant u\leqslant 2\pi$ with $0\leqslant\varepsilon\leqslant 2/\pi$. Its graph is the two inner curves in Fig. 12. Using this graph, given $0\leqslant\varepsilon\leqslant 2/\pi$, we

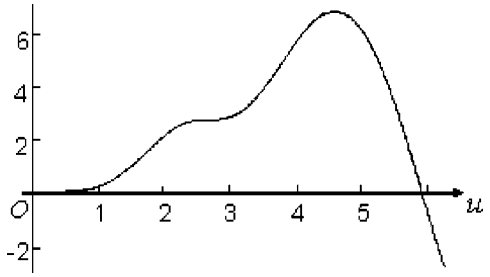

FIG. 11. Plot of the left side of Eq. (7.4) for $\rho=1+(15/41)\cos(5s/4)$ with $s_1=0$, $s_2=u\leqslant 2\pi$.

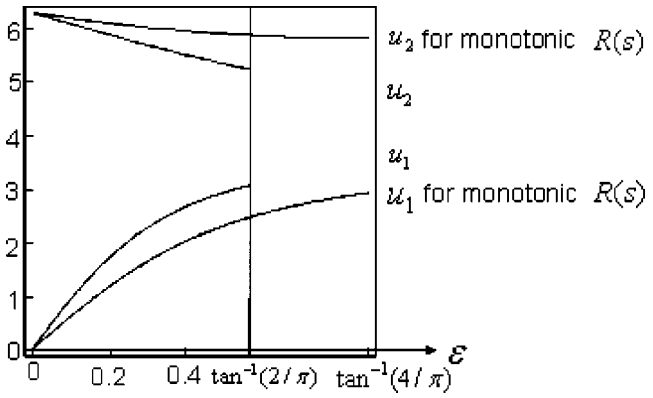

FIG. 12. Relation between ε and u_1, u_2.

can find u_1 from the lower curve and u_2 from the top curve. When Eq. (9.1) or equivalently Eq. (9.2) is satisfied for all $s\in[a,b]$, Eq. (7.4) holds for $u_1\leqslant s_2-s_1\leqslant u_2$.

In other words, for any given s_1, there is a fan-shaped surface consisting of PI lines from the point on the 3D spiral at $s=s_1$ to points at $s=s_2$, with $u_1\leqslant s_2-s_1\leqslant u_2$. When s_1 moves upward, this fan-shaped surface also moves upward along the 3D spiral. The 3D region passed by, or actually consisting of, these fan-shaped surfaces, is a region inside the 3D spiral in which any point is passed by one and only one PI line, when there is a bound $\varepsilon\leqslant\pi/2$ for $R'(s)/R(s)$, or equivalently a bound $\tan^{-1}\varepsilon$ for $|\omega-\pi/2|$.

X. UNIQUE PI-LINE REGION FOR MONOTONIC $R(s)$

If the function $R(s)$ is monotonic, then $R'(s_1)/R(s_1)$ and $R'(s_2)/R(s_2)$ are of the same sign. Therefore if Eq. (9.1) holds, i.e., if the angle ω is bounded by Eq. (9.2), we get an inequality better than Eq. (9.3):

$$\left(\sqrt{\frac{R(s_1)}{R(s_2)}}-\sqrt{\frac{R(s_2)}{R(s_1)}}\right)^2+4+\pi\left(\frac{R'(s_1)}{R(s_1)}-\frac{R'(s_2)}{R(s_2)}\right)$$
$$\geqslant 4-\varepsilon\pi. \tag{10.1}$$

Consequently, if $\varepsilon=4/\pi$ i.e., if

$$\left|\omega-\frac{\pi}{2}\right|\leqslant\tan^{-1}\frac{4}{\pi}\cong 0.905\cong 51.85°, \tag{10.2}$$

Eq. (7.4) holds for any point $(0,0,z_0)$.

A smaller ε in Eqs. (9.1) and (9.2) will also give us a larger region with PI line uniqueness. Given $\varepsilon\leqslant 4/\pi$ with Eq. (9.1) or equivalently Eq. (9.2), Eq. (7.4) holds if

$$2-2\cos u-u\sin u-\varepsilon|\sin u-u\cos u|-\varepsilon^2 u\sin u\geqslant 0. \tag{10.3}$$

Note that the coefficient of ε is different from that in Eq. (9.5). Since $R'(s_1)/R(s_1)$ and $R'(s_2)/R(s_2)$ are of the same sign, there is no need to have an absolute sign for the last term in Eq. (10.3). Solving its equality for ε, we get

$$\varepsilon = \frac{1}{2u \sin u}\left(-|\sin u - u\cos u| + \sqrt{(\sin u - u\cos u)^2 + 4u \sin u(2 - 2\cos u - u \sin u)}\right) \tag{10.4}$$

for $0 \leqslant u \leqslant 2\pi$ with $0 \leqslant \varepsilon \leqslant 4/\pi$. Its graph is the two outer curves in Fig. 12. Using this graph, given $0 \leqslant \varepsilon \leqslant 4/\pi$, we can find u_1 from the lowermost curve and u_2 from the topmost curve. Note that this region is larger than the one in Sec. IX. When Eq. (9.1) or equivalently Eq. (9.2) is satisfied for all $s \in [a,b]$, Eq. (7.4) holds for $u_1 \leqslant s_2 - s_1 \leqslant u_2$. The corresponding region in which any point is passed by a unique PI line can be constructed using these u_1 and u_2 as in Sec. IX.

XI. DISCUSSION AND CONCLUSION

In our earlier work on variable pitch helical cone-beam scanning, we suggested an extension of the Tam–Danielsson detection window, and established the PI line existence and uniqueness.[15] Then, we pointed out that that a Katsevich-type formula may be established in that variable pitch case in the Grangeat or Tuy frameworks.[6,16] Similar to what was contemplated there, we will proceed to construct a Katsevich-type cone-beam reconstruction algorithm in the proposed variable radius spiral scanning cases. Note that when the PI line is not unique a Katsevich-type formulation is still possible,[17] but nontrivial handling of a weight function and optimal design of a data featuring technique will become necessary in a general case.

The concepts of the PI line and the Tam–Danielsson window are theoretically critical in the derivation of the Katsevich-type filtered backprojection algorithms, in which the data redundancy must be one. However, by the Katsevich method filtering paths are not always contained in the Tam–Danielsson window, which provides an opportunity for us to utilize the data redundancy. Our group has made significant progress along this direction, and will report our results soon.[18]

The exact cone-beam reconstruction may be formulated in different ways.[5–7,16] In the special case of spiral cone-beam geometry, the formulation based on the PI line and the associated Tam–Danielsson window is advantageous for its geometric interpretation (similar to that for Orlov theorem[13]), explicit link to the minimum data requirement (defined by the Tam-Danielsson window), and implicit treatment of the weighting function (always one hence no need for feathering). However, such a formulation seems imperfect. First, its asymmetry in the scanning geometry relative to a given pixel might indicate possible optimization. Also, its detection coverage (either traditional or generalized Tam–Danielsson windows) may be systematically redesigned to allow practical flexibilities and meet image quality requirements. Finally, we should explore schemes not limited by the concepts of PI line and Tam–Danielsson window, which may be more fundamental and effective for our nonstandard spiral cone-beam CT problem.

In conclusion, we have formulated a generalized Tam–Danielsson window in the case of variable radius spiral cone-beam scanning, studied the existence and uniqueness of the PI line with such a 3D spiral scan, and established a theoretical foundation for exact reconstruction applicable to our proposed spiral cone-beam electron-beam CT/micro-CT.[19]

ACKNOWLEDGMENTS

This work is partially supported by a Carver Scientific Research Initiative grant and an NIH/NIBIB grant (EB002667).

[a]Electronic mail: yangbo-ye@uiowa.edu

[1] D. P. Boyd and M. J. Lipton, "Cardiac computed tomography," Proc. IEEE **71**, 298–307 (1983).
[2] G. Wang, C. R. Crawford, and W. A. Kalender, "Multi-row-detector and cone-beam spiral/helical CT," IEEE Trans. Med. Imaging **19**, 817–821 (2000).
[3] G. Wang and M. W. Vannier, "Overview on micro-CT scanners for biomedical applications," Adv. Imaging Electron Phys. **16**, 22–27 (2001).
[4] G. Wang, T. H. Lin, P. C. Cheng, D. M. Shinozaki, and H. G. Kim, "Scanning cone-beam reconstruction algorithms for x-ray microtomography," Proc. SPIE **1556**, 99–112 (1991).
[5] A. Katsevich, "Theoretically exact filtered backprojection-type inversion algorithm for Spiral CT," SIAM (Soc. Ind. Appl. Math.) J. Appl. Math. **62**, 2012–2026 (2002).
[6] A. Katsevich, "A general scheme for constructing inversion algorithms for cone beam CT," Int. J. Math. Math. Sci. **21**, 1305–1321 (2003).
[7] A. Katsevich, "An improved exact FBP Algorithm for spiral CT," Adv. Appl. Math. **32**, 681–697 (2004).
[8] G. Wang, T. H. Lin, P. C. Cheng, and D. M. Shinozaki, "A general cone-beam reconstruction algorithm," IEEE Trans. Med. Imaging **12**, 486–496 (1993).
[9] K. C. Tam, S. Samarasekera, and F. Sauer, "Exact cone beam CT with a spiral scan," Phys. Med. Biol. **43**, 1015–1024 (1998).
[10] P. E. Danielsson, P. Edholm, J. Eriksson, and S. M. Magnusson "Towards exact reconstruction for helical cone-beam scanning of long object. A new detector arrangement and a new completeness condition," Proceedings of the 1997 Meeting on Fully 3D Image Reconstruction in Radiology and Nuclear Medicine, Pittsburgh, PA, 1997, edited by D. W. Townsend and P. E. Kinahan, pp. 141–144.
[11] M. Defrise, F. Noo, and H. Kudo, "A solution to the long-object problem in helical cone-beam tomography," Phys. Med. Biol. **45**, 623–643 (2000).
[12] K. C. Tam, "Three-dimensional computerized tomography scanning method and system for large objects with small area detector," US patent 5,390,112, 1995.
[13] S. S. Orlov, "Theory of three-dimensional reconstruction. I. Conditions for a complete set of projections," Sov. Phys. Crystallogr. **20**, 312–314 (1975); "Theory of three-dimensional reconstruction. II. The recovery operator," *ibid.* **20**, 429–433 (1975).
[14] Y. Zou and X. Pan, "Exact reconstruction from minimum data in helical cone-beam CT," Radiology **229**, 168 (2003).
[15] Y. Ye, J. Zhu, and G. Wang "Minimum detection windows, PI-line existence and uniqueness for helical cone-beam scanning of variable pitch," Med. Phys. **31**, 566–572 (2004).
[16] G. H. Chen, "From Tuy's inversion scheme to Katsevich's inversion scheme: Pulling a rabbit out of the hat," Proceedings of the 2003 Meeting on Fully 3D Image Reconstruction in Radiology and Nuclear Medicine, 2003.
[17] J. D. Pack, F. Noo, and H. Kudo, "Investigation of a saddletrajectory for cardiac CT imaging in cone beam geometry," Proceedings of the 2003 Meeting on Fully 3D Image Reconstruction in Radiology and Nuclear Medicine, 2003.
[18] S. Y. Zhao, H. Y. Yu, and G. Wang, "A family of Katsevich-type FBP algorithms for spiral cone-beam CT," Proc. SPIE (to be published).
[19] G. Wang and Y. Ye, "Nontrivial spiral cone-beam scanning methods, apparatus, and applications," Patent disclosure filled with University of Iowa, November 2003 (US provisional patent application pending).